GEOPHYSICAL RESEARCH LETTERS, VOL. 29, NO. 24, 2182, doi:10.1029/2002GL015611, 2002

Complex images of Moho and variation of Vp/Vs across the Himalaya and South Tibet, from a joint receiver-function and wide-angle-reflection approach

A. Galvé,[1,4] M. Sapin,[1] A. Hirn,[1] J. Diaz,[2] J.-C. Lépine,[1] M. Laigle,[1] J. Gallart,[2] and M. Jiang[3]

Received 5 June 2002; revised 13 September 2002; accepted 23 September 2002; published 24 December 2002.

[1] Teleseismic receiver functions (RF) allow us to image the spatial variation of the crust-mantle boundary (Moho) along a tight array spanning from south of the Himalayas to the centre of the Tibetan Plateau. This approach is cross-tested with wide-angle reflection imaging (WARR). Highlighted by each of the two independent methods, a complex architecture of the Moho with dipping and overlapping segments indicating lithospheric imbrication, is confirmed. The joint use of the two methods reveals an increase of the average crustal P-to-S-wave-velocity ratio from south to the centre of the Lhasa block. This may be due to lowered S-wave velocity confined in specific layers, that may be interpreted as partial melt. This accounts for half of the relative increase in the delay of direct teleseismic S-wave arrivals with respect to P-wave arrivals from south to north, suggesting a similar anomaly in the shallower mantle. *INDEX TERMS:* 0935 Exploration Geophysics: Seismic methods (3025); 7218 Seismology: Lithosphere and upper mantle; 9320 Information Related to Geographic Region: Asia. **Citation:** Galvé, A., M. Sapin, A. Hirn, J. Diaz, J.-C. Lépine, M. Laigle, J. Gallart, and M. Jiang, Complex images of Moho and variation of Vp/Vs across the Himalaya and South Tibet, from a joint receiver-function and wide-angle-reflection approach, *Geophys. Res. Lett.*, *29*(24), 2182, doi:10.1029/2002GL015611, 2002.

1. Introduction

[2] Along a transect across the Himalayas and southern Tibet, wide-angle reflection and refraction seismic (WARR) early experiment suggested lateral heterogeneity at depth, with complex structure of the Moho [*Hirn et al.*, 1984a, 1984b]. This Moho marker has not been sampled since then over a great length, by several surveys that have brought a great amount of insight into other aspects [*Zhao et al.*, 1993; *Brown et al.*, 1996; *Makovsky et al.*, 1999; *Hauck et al.*, 1998]. *Kind et al.* [1996] did not resolve Moho depth variations in the Lhasa block but their receiver-functions were widely spaced. *Zhao et al.* [2001] constructed a model with an essentially flat Moho from the northern Lhasa block into the Qang Tang area by using a recent cross-strike WARR experiment.

[3] To compare to the early WARR transect, we report here the sampling of the Moho with a seismic dataset of completely different nature and geometry. A new set of teleseismic receiver-functions, RF, was obtained and processed specifically in order to achieve structural profiling with a horizontal and vertical resolution appropriate to be compared to WARR.

2. Complex Moho Architecture

[4] We deployed in 1992 24 broad-band 3-component stations at 25 km intervals from Nepal, south of the High Himalayas, into the Qang Tang block in Central Tibet (Figure 1). Here, the data of this array have been processed to obtain the image of interfaces that convert the incoming teleseismic P waves to SV waves. We have adopted the processing and display schemes designed by *Kosarev et al.* [1999] who discuss mantle variations using another dataset obtained from a much coarser network spanning over Tibet. We can focus here better on the Moho because a reasonable cross-sampling and resolution up to shallow depth is achieved with our more homogeneous and relatively dense array between Nepal and Qang Tang. The WARR section of Figure 2a arised from explosion seismology of the 1981–82 experiment [*Hirn et al.*, 1984a, 1984b; *Sapin et al.*, 1985; *Sapin and Hirn*, 1997]. Figure 2b displays the structural transect of the RF. The general styles of Moho architecture are similar, documenting that the imaged structure is indeed real because the data are independent and of completely different nature. If the Moho were flat but changes in WARR arrival times due to Vp variations, RF would also give a flat Moho since the delay of the converted on the direct wave depends on Moho depth and on the difference in P and S slownesses but only weakly on Vp in the crust. Since the RF Moho is not flat, it constrains the WARR arrival time variation to be indeed due to Moho topography rather than crustal Vp variation.

[5] In comparing the overall architecture of the sections in the Moho depth range of 50 to 90 km indicated by WARR (Figure 2a), we begin to discuss the section between the High Himalayas (HH) and the Indus-Tsang Po suture (ITS) where an E-W reversed strike-line identifies segment 3 as Moho at 70 km depth. The RF section shows consistently a strong converting interface with positive polarity (Figure 2b). Under the Himalaya and further south, two south dipping converters, 1 and 2, are

[1]Laboratoire de Sismologie Expérimentale, Dpt Sismologie UMR 7580, Institut de Physique du Globe de Paris, 4 place Jussieu, Paris, France.
[2]Dpt de Ciencias de la Terra IJA, CSIC, calle Lluis Sole i Sabaris, Barcelona, Spain.
[3]Chinese Academy of Geological Sciences, Baiwanzhuang road, Beijing, China.
[4]Now at School of Earth Sciences, Victoria University of Wellington, New Zealand.

0094-8276/02/2002GL015611

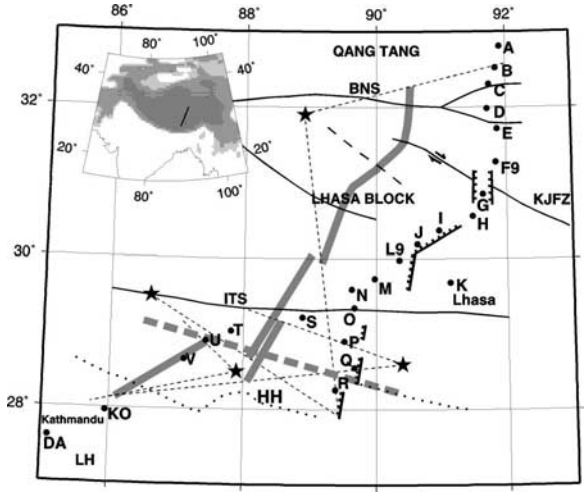

Figure 1. Sketch map of southern half of Tibet and Himalayas with layout of transects of RF and WARR: Teleseismic stations (dots with lettering) [*Hirn et al.*, 1995, 1997, 1998], are used here for RF. Along the same road receivers were deployed more tightly for WARR [*Hirn et al.*, 1984b] and recorded broadside shots (stars) within the range indicated by dotted lines, at offsets adequate for Moho reflections which sampled the subsurface at mid points (gray lines). Shots were also recorded on an inline profile (dashed gray line). ITS = Indus-Tsangpo suture, LH = Lesser Himalaya, HH = High Himalaya, KJFZ = Karakorum-Jiali fault zone, BNS = Banggong Nujiang suture.

clearly imaged, above the flat Moho converter 3 south of the ITS mentioned above. This system of three converters coincides with the explosion seismology image of a system of three reflectors which can be interpreted to be segments of the Moho according to their large amplitude at large offsets from the shots. At the ITS, a change to north dipping of the deep crustal or Moho interfaces is established for converter 4. Converters 5 and 6 under the southern Lhasa block begin at shallower depth than converter 3. Several north dipping and overlapping reflectors are seen in the WARR image, consistently with the converters in the RF image. The RF images better the deeper part of converter 4, whereas where the Moho reflector segments get superposed, the WARR image of deeper ones is weakened. This is expected because the critical distance of deeper large-amplitude reflections is increased to larger offsets and the overlying Moho reflectors partly screen off energy. The superposition of converters, like 4 and 5 with similar characters indicating that they may be Moho segments, would imply that those have been transported over one another.

[6] There is some heterogeneity at shorter spatial scale, like the one imaged as a step from segment 9 to 10 in the WARR. This could alternatively be due to a lateral contrast in crustal composition. In any case there is a structural anomaly located close to the Banggong-Nujiang Suture (BNS). *Hirn et al.* [1984b] suggested therefore that these features are related with each other. The RF section displays sharp changes, for instance in a similar position as the one inferred from the WARR near the BNS. This feature binning heterogeneous data, since it is consistently seen in partial views of receiver-gather (Figure 2d) or different receivers and different back-azimuths (Figures 2e and 2f). Since the sampled elements are over 100 km apart laterally, the overall agreement of the RF feature with the image of the WARR does not however provide an unequivocal evidence for the reality of such structures.

3. Composition and Physical State Variation

[7] Since the specific characters of the two sections agree generally and hence can be attributed to the same structural elements, the corresponding interfaces should be precisely placed at the same location and depth in both sections. The first fit achieved is the correspondence of the two sections in horizontal direction. South of the ITS, the two datasets cover grossly the same region, but to the North, the WARR Moho sampling is obtained 100 km west of the line of RF stations. The projection of the two images on each other, as in Figures 2a and 2b, assumes that the structural strike at depth is E-W, like the one of the sutures ITS and BNS. However, this may not be the best choice since the Karakoram-Jiali Fault Zone (KJFZ) in the Lhasa block [*Armijo et al.*, 1989] appears younger and active. One of its segments with N 150°E strike crosses the two transects at different latitudes, from close to the BNS in the west on the WARR transect, to almost midway between ITS and BNS on the RF transect. The projection of the observations of the WARR transect along this direction onto the RF transect (Figure 2 insert of WARR segment under RF transect) results in a better coincidence of the structural images.

[8] The matching in depth between WARR and RF sections brings constraints for the velocities used for transforming the time sections to same depth in each image. WARR reversed strike-lines constrain average Moho depth along the transect to vary between 50 and-90 km. For backprojection and time-depth conversion of the RF we take accordingly on top a velocity with a crustal value down to 50 km depth and a gradient so that mantle velocity is reached at 90 km depth. With this velocity model and a standard Vp/Vs = 1.73, the depth of the WARR and RF images are brought into reasonable agreement in the southern third of the transects. Keeping the same velocity values to migrate RF data North of the ITS would bring the converting interfaces significantly deeper than WARR reflectors, by up to 8 km. Since Vp must be the same as that one derived from WARR and used for its depth transformation, the only way to match the RF depths to the shallower WARR reflector in the north is to decrease there the average S velocity in the crust. A constant Vp but decreasing Vs northward, that is increasing Vp/Vs from 1.73 south of ITS to 1.85 average in 50 km thickness of the crust, in the middle of the Lhasa block to the end of the section, brings Moho depths to coincidence in Figure 2. This also allows to account partly for another type of observation, which is that delay times of first arrival teleseismic P-waves decrease northwards while those of S-waves increase strongly with respect to any global model. *Hirn et al.* [1997] suggested earlier a northward decrease of total thickness of the crust midway in the Lhasa block, and decrease of its average S velocity northward of ITS. The WARR and RF images of the Moho

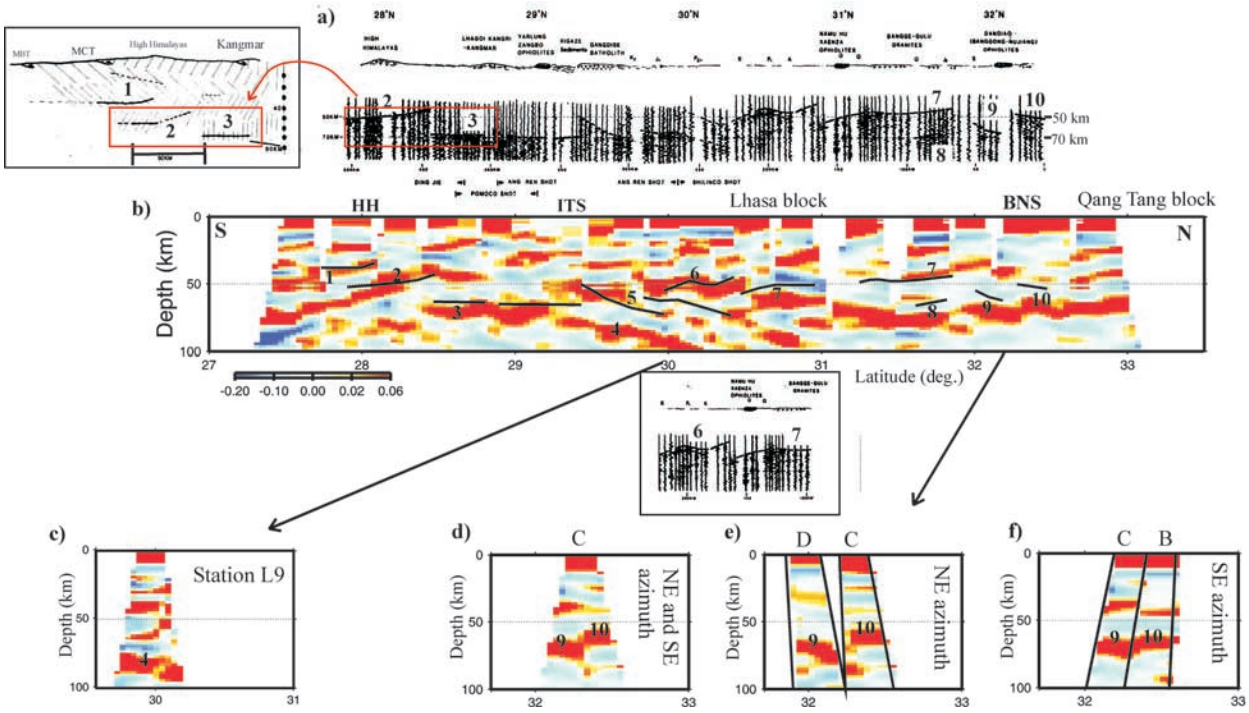

Figure 2. Structural sections of WARR and RF through Himalayas-Tibet. (a) WARR is displayed as a N-S approximate-depth section of Moho reflections, with depth marks at 50 and 70 km. The section was obtained by local normal-move out correction of wide-angle reflections to constant offset for crustal Vp of 6.25 km/s. Sketch at extreme left completes section by interface segment 1 obtained in a different geometry [after *Hirn et al.*, 1984a, 1984b]. Also part of the section with segments 6 and 7 is re-plotted as an inset under the RF section in a projection with the N 150°E strike of the KJFS, instead of E-W. (b) RF transect, 450 traces at 24 receivers. Velocity model described in text. The reflectors observed on the WARR section are superposed on this section (black lines) (c) Single-station image showing dip of converter segment 4. (d) Segments 9 to 10 with discontinuity seen on gather of single station C. (e) Same as (d), but for waves coming with back-azimuths only in the NE quadrant, at stations C and D. (f) Same as (e), but for different, SE back-azimuths and different stations, C and B.

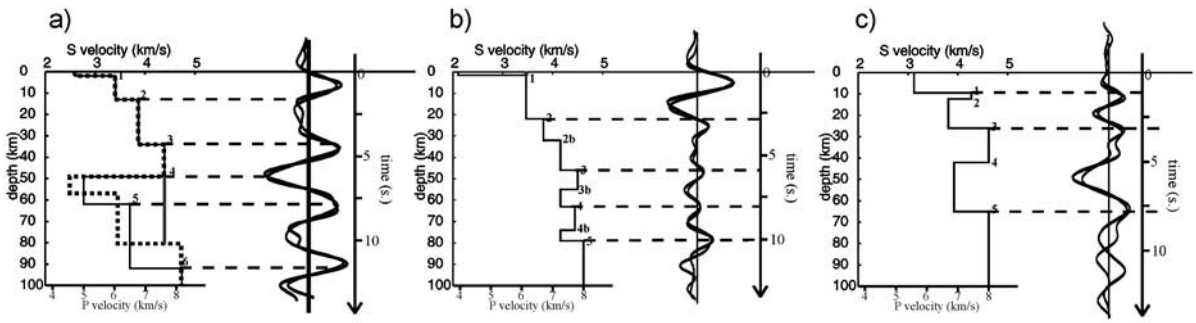

Figure 3. Right columns: RF, receiver-functions derived from observations (dark line), and models (gray line), that appear in left columns. (a) Station G. Black line on the velocity model corresponds to constant velocity ratio of 1.73. Matching the WARR and RF images required an anomalously low Vs and a higher Vp/Vs. RF modelling constrains the higher than standard velocity ratio which suggests presence of partial melt, in the deep layer (between 50 and 80 km depth). Simplest case here keeps same Vp as in the layer above (gray line in model) which yields new Vs (dotted line in model) and shallower depth for base of low-velocity layer. The RF synthetics (in gray) for the two models are undistinguishable in this time window at this scale. (b) Station E in the northern Lhasa block. RF with alternating high and low-velocity layers modelled from 45 to 80 km depth. (c) Station T just south of ITS. First positive swing that is late but strong modelled as due to layer of high-velocity with respect to continental crust, possibly in correspondence with ophiolites [*Makovsky et al.*, 1999].

topography together with the change in crustal Vp/Vs confirm this explanation. In addition, the effect of crustal Vs reduction would amount to a 1-second increase northward of the relative delay of direct teleseismic S-waves with respect to P-waves. Since a twice larger anomaly was observed, the shallow mantle contains in this model a Vs change of same strength from south to north as that one in the crust.

[9] The velocity-depth model cannot be derived uniquely from the observed receiver-function signal, as it is well-known. Forward modelling tests in Figure 3 consider the simplest velocity-depth functions, i.e. with a minimum number of interfaces with a first-order velocity discontinuity. Although this type of model tends to produce largest internal multiples, which are computed, each peak in the observed RF, in particular positive, corresponds to a primary conversion, i.e. marks an interface. Conversely, this supports the assumption that the section of Figure 2b may be regarded as an image of real interfaces. North of the ITS, RF exhibit unusually strong negative peaks, e.g. station G in Figure 3a, from which presence of partial melt within the crust is in agreement with *Kind et al.* [1996]. Station E (Figure 3b) shows a less extreme low-velocity part in the deeper pile of layers of alternating high and low velocities, but high-velocity layers need to reach mantle velocities, consistently with the independent WARR analysis of reflection amplitude that suggested superposed Moho segments.

4. Conclusions

[10] We have used here the RF method on a tight linear array through the Himalayas and southern Tibet. The spatial resolution of the resulting images allows comparison with the image of reflectors, mainly for the Moho, previously imaged by WARR. The two methods and datasets are completely independent. The two images exhibit generally strong similarities. The cross-check provided by the two images thus lends credence to the reality of these sections with respect to the complexity of the crustal architecture. Principal types of models proposed for the evolution of Himalaya-Tibet, do not predict Moho otherwise than being continuous and smooth. Instead the Moho appears here as being made of a series of segments that dip, overlap or superpose each other. Here we confirm the occurrence of separate tectonic thickening of brittle layers at upper crustal level on one side and at the Moho level on the other side, with decoupling in between and beneath [*Hirn et al.*, 1984a]. The match of the RF and WARR images of the architecture, when converting the time-sections to depth sections constrains the velocity field. Principally, it proves S-wave low-velocity layers within the crust north of ITS. This joint approach therefore puts constraints on physical state and composition of the thickened crust. The northward increase of the relative delay of teleseismic S-wave with respect to P-wave residuals is consistent with the spatial variation of the crustal Vp/Vs-ratio determined from RF and WARR but about twice as large. This suggests that in the shallow mantle there is an increase of the Vp/Vs-ratio giving about the same effect as that one in the crust.

[11] **Acknowledgments.** Fieldwork has been supported by the French INSU-CNRS and the Chinese MGMR. R. Kind is thanked for hospitality to bring RF processing to common standard. Thanks also to Walter Mooney, Ewald Lueschen and reviewers for their constructive criticism.

References

Armijo, R., et al., Late cenozoic right-lateral strike-slip faulting in southern Tibet, *J. Geophys. Res.*, *94*, 2787–2838, 1989.

Brown, L. D., et al., Bright spots, structure, and magmatism in southern Tibet from INDEPTH seismic reflection profiling, *Science*, *274*, 1688–1690, 1996.

Hauck, M. L., et al., Crustal structure of the Himalayan orogen at 90° east longitude from Project INDEPTH deep reflection profiles, *Tectonics*, *17*, 481–500, 1998.

Hirn, A., Features of the crust-mantle structure of Himalayas-Tibet: A comparison with seismic traverses of Alpine, Pyrenean and Variscan orogenic belts, *Phil. Trans. R. Soc. Lond., A*, *326*, 17–32, 1988.

Hirn, A., et al., Crustal structure and variability of the Himalayan boarder of Tibet, *Nature*, *307*, 23–25, 1984a.

Hirn, A., et al., Lhasa block and bordering sutures, A continuation of a 500 km Moho traverse through Tibet, *Nature*, *307*, 25–28, 1984b.

Hirn, A., et al., Seismic anisotropy as an indicator of mantle flow beneath the Himalayas and Tibet., *Nature*, *375*, 571–574, 1995.

Hirn, A., et al., Increase in melt fraction along a south-north traverse below the Tibetan Plateau, evidence from seismology, *Tectonophysics*, *273*, 17–30, 1997.

Hirn, A., et al., Variation of shear wave residuals and splitting parameters from array observations in Southern Tibet, *PAGEOPH*, *151*, 407–431, 1998.

Kind, R., et al., Evidence from earthquake data for a partially molten crustal layer in southern Tibet, *Science*, *274*, 1692–1694, 1996.

Kosarev, G., et al., Seismic evidence for a detached Indian lithospheric mantle beneath Tibet, *Science*, *283*, 1306–1309, 1999.

Makovsky, Y., et al., Midcrustal reflector on reflector on INDEPTH wide-angle profiles: An ophiolitic slab beneath the India-Asia suture in southern Tibet?, *Tectonics*, *18*, 793–808, 1999.

Sapin, M., and A. Hirn, Seismic structure and evidence for evolution of the crust in the Himalayan convergence, *Tectonophysics*, *273*, 1–16, 1997.

Sapin, M., et al., A seismic sounding in the crust of Lhasa block, Tibet, *Ann Geophys.*, *3*, 637–648, 1985.

Zhao, W.-J., K. D. Nelson, and Project INDEPTH Team, Deep seismic reflection evidence for continental underthrusting beneath southern Tibet, *Nature*, *366*, 557–559, 1993.

Zhao, W., et al., Crustal structure of central Tibet as derived from project INDEPTH wide-angle seismic data, *Geophys. J. Int.*, *145*, 486–498, 2001.

A. Galvé, M. Sapin, A. Hirn, J.-C. Lépine, and M. Laigle, Laboratoire de Sismologie Expérimentale, Dpt Sismologie UMR 7580, Institut de Physique du Globe de Paris, 4 place Jussieu, Paris 75005, France.

J. Diaz and J. Gallart, Dpt de Ciencias de la Terra IJA, CSIC, calle Lluis Sole i Sabaris, Barcelona 08028, Spain.

M. Jiang, Chinese Academy of Geological Sciences, Baiwanzhuang road, Beijing, China.